Charge redistribution and electronic behavior in a series of Au-Cu alloys

M. Kuhn and T. K. Sham
Department of Chemistry, University of Western Ontario, London, Canada N6A 5B7
(Received 15 July 1993)

A series of Au-Cu alloys of various stoichiometries and order have been studied using x-ray photoemission spectroscopy (XPS) and x-ray absorption spectroscopy (XAS). Significant electronic changes are associated with alloying and with changes in the local environment. The Au 5*d* electron charge depletion has been determined independently from XPS core-level and Mössbauer isomer shifts and from x-ray absorption near-edge structure (XANES) measurements. Strong correlations were found using both methods in the parameters investigated here, especially in the elucidation of the charge-transfer mechanism. It is found that at the Au site there is a loss of *d* charge, upon alloying, which increases as Au becomes more dilute in Cu. This along with XANES evidence of *d* charge gain at the Cu site, conduction (primarily 6*s*) charge gain at the Au site, and overall charge gain at the Au site verifies the charge compensation model in which Au loses *d* charge but is overcompensated by a gain of conduction charge. This observation is in line with electronegativity (Au is more electronegative than Cu) and electroneutrality (the overall gain of charge is small) arguments. It is also found that there is a strong linear correlation between the 5*d* hole count at the Au site and (1) the Mössbauer isomer shift, (2) alloy *d*-band width, (3) "Au" apparent spin-orbit splitting in the alloy *d* band. By comparing the ordered and disordered species (which have different local environments) it is found that the charge transfer depends primarily on the local environment (coordination number of like and unlike atoms) and not on atomic separation. The charge transfer (*d*-band depletion) was larger in the ordered species and can be explained by the number of Cu and Au nearest neighbors as compared to the disordered phases.

I. INTRODUCTION

Charge transfer and *d*-*d* interactions in noble-metal alloys have generated considerable interest and debate in recent research. Noble-metal alloys, such as Au-Cu and Au-Ag, are considered prototypes for investigating interactions of metals with full *d* bands and Friedel screening. The Au-Cu system is also a classical example of order-disorder transitions with superlattice phases around the stoichiometric compositions $Cu_{0.75}Au_{0.25}$, $Cu_{0.5}Au_{0.5}$, and $Au_{0.75}Cu_{0.25}$ (henceforth denoted Cu_3Au, AuCu, and Au_3Cu, respectively).[1,2]

This paper will examine a variety of issues concerning a series of Au-Cu alloys [Au_3Cu (order and disorder), AuCu (order and disorder), Cu_3Au (order and disorder), $Cu_{0.875}Au_{0.125}$, and $Cu_{0.95}Au_{0.05}$]: the charge transfer, the interaction between the Au and Cu *d* bands, and the effect of local structure on the electronic structure for the ordered and disordered phases of these alloys. Au is the most electronegative of metallic elements, and therefore upon alloying with Cu, for example, an overall transfer of charge from the Cu site to the Au site is expected. This overall charge transfer, however, must be small to preserve electroneutrality required by metallic systems. Previously reported positive ^{197}Au Mössbauer isomer shifts[3,4] do show an increase of contact density at the nucleus in Au alloys relative to pure Au, yet positive Au 4*f* binding energy shifts indicate an apparent depletion of charge at the Au site (shown below), not only for the Au-Cu system, but also for a variety of other Au intermetallics.[4–11] These same trends have also recently been observed for Au_x-Ag_y (Ref. 12) alloys and other Au intermetallics (such as Au_x-Ti_y and Au_x-Ta_y alloys).[13,14] Surface studies of Au-Cu and Au-Ag on Ru(001) also show a positive binding energy shift relative to pure Au.[15,16] A charge compensation model[6] has often been used to explain these apparent inconsistencies, that is, that upon alloying Au loses *d* charge, but is overcompensated by a gain of mainly *s*-*p* charge from Cu. Because of the larger screening effect from the *d* electrons, their loss leads to a higher effective Coulombic potential for the remaining electrons, thereby causing a positive 4*f* binding energy shift. In addition, the overcompensation of *s*-*p* charge gives the Au site an overall gain of charge in line with electronegativity arguments.

Much debate has occurred as to the nature and the extent of the Au and Cu *d*-band interactions in both experiment and theory (calculations), especially in the case of Cu_3Au.[10,17–28] In 1962 Catterall and Trotter[17] published work supporting the idea that the alloy *d* band is merely a supposition of the respective *d*-band components. Since then, both the localized[10,20,25,26] and mixed-band[17–19,21] views have had experimental support with theoretical methods (calculations) indicating some overlap but with reasonably well-defined "Au" and "Cu" regions.[22,23,27,28] The localized approach is sometimes referred to as the *d*-*d* repulsion model[10,11] and can be viewed as the repulsive overlap due to alloying, separating the constituent *d* bands. The mixed-band view, on the other hand, points to extensive *d*-band mixing, results in the loss of well-defined "Au" and "Cu" regions in the valence band. It has also been shown by calculations (not as much so by experiment) that the order-disorder transition has an

effect on the valence-band features exhibited by these d states.[22–24,28] To decipher the contributions of the components to the alloy d band, the nature of the apparent splitting of the higher-binding-energy side of the band and the changes in overall d-band widths with compositional changes and order-disorder transitions must be understood.

In this paper, both the Au $4f$ and Cu $2p$ core levels and the valence bands that were probed using x-ray photoelectron spectroscopy (XPS) are reported. The analysis includes determining binding energy shifts, apparent d-band splitting, alloy d-band widths, and charge-transfer counts at the Au site upon alloying from Mössbauer and XPS results.

We have also studied the near-edge absorption regions of these alloys at the Au $L_{2,3}$ and Cu K edges. From previous experiments,[29–36] it has been found that x-ray adsorption near-edge structure (XANES) exhibits sensitivity to small changes in the electronic configuration upon alloying. Both Au and Cu have nominally full d bands, and thereby, small changes in the occupied density of states are not easily detected by photoemission, whereas small changes in the unoccupied density of states become readily apparent in Au $L_{2,3}$- and Cu K-edge XANES measurements.

Using the charge compensation model of Watson, Hudis, and Perlman,[6] the d-charge-transfer count (Δn_d), the non-d-conduction-charge transfer of primarily $6s$ character (Δn_c), and the overall charge transfer at the Au site ($\delta = \Delta n_d + \Delta n_c$) will be determined from XPS Au $4f$ shifts and Mössbauer isomer shifts. The change in d-hole count (Δh_t) will also be independently determined via XANES analysis. The XANES-derived Δh_t and Mössbauer isomer shifts will be used to establish a Δh_t versus Δn_c correlation. A direct comparison will also be made between the XANES-derived d-hole count Δh_t and the XPS- and Mössbauer-derived d-charge transfer Δn_d. A further comparison will be made between the XANES-derived hole count and valence-band features, namely, the alloy d-band width and the "Au" $5d$ spin-orbit splitting. The impact of the local environment (coordination number and interatomic distance) to charge transfer will be examined as a function of the composition of the alloy and upon ordering for Au_3Cu, AuCu, and Cu_3Au.

The rest of the paper is organized as follows: The experimental procedure is described in Sec. II followed by the results in Sec. III. A number of issues are discussed in Sec. IV, and conclusions are given in Sec. V.

II. EXPERIMENTAL DETAILS

Foils of various Au-Cu alloys (atomic compositions 5.0–95.0, 12.5–87.5, 25.0–75.0, 50.0–50.0, and 75.0–25.0 at. %) were prepared from 99.9% pure metals. Accurately weighed amounts were melted under H_2 at about 1500 K in boats made of pure silica. Each melt, while kept in rapid motion, was quenched under H_2. The ingots were rolled into foils with a thickness of about one absorption length (0.3 mil) at the Au L_3 edge. Under these conditions, Cu_3Au, AuCu, and Au_3Cu exist in their disordered states. Further preparations were done on the Cu_3Au, AuCu, and Au_3Cu samples by annealing in an evacuated quartz tube for 2 weeks at just below the transition temperature for their respective stoichiometric compositions (i.e., 493 K for AuCu and 435 K for Au_3Cu), as indicated by the Au-Cu phase diagram, to achieve their respective ordered states. The degree of order and disorder was checked with both Cu K- and Au L_3-edge extended x-ray absorption fine structure (EXAFS). In general, the disordered samples exhibited less frequent and weaker oscillations (Fig. 1).[37]

Both the annealed Cu_3Au and Au_3Cu alloys form an ordered cubic $L1_2$ structure, while under the aforemen-

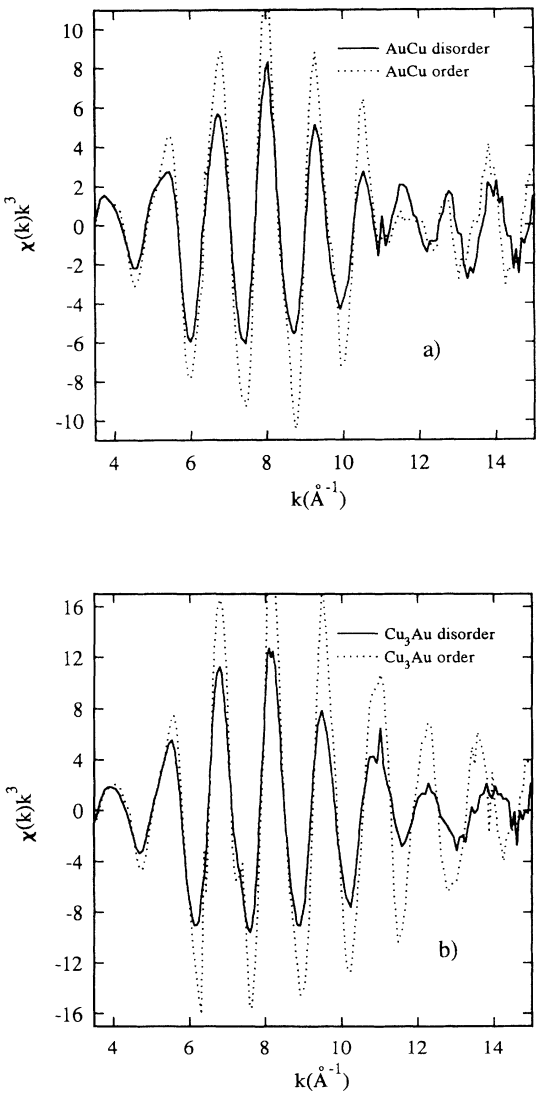

FIG. 1. EXAFS of (a) AuCu order-disorder alloys (upper panel) and (b) Cu_3Au order-disorder alloys (lower panel). The EXAFS spectra were normalized to the edge jump of one atom and then truncated 40 eV to approximately 1000 eV above the Au L_3 threshold at 11 917 eV. A linear background subtraction was done, then a conversion to k space, followed by a third-order spline (three sections) subtraction. The amplitudes are directly comparable.

tioned conditions the AuCu alloy forms an ordered tetragonal $L1_0$ type of structure (denoted by AuCu I). There also exists a higher-temperature ordered phase denoted by AuCu II. $Cu_{0.875}Au_{0.125}$ and $Cu_{0.95}Au_{0.5}$ do not form superlattice structures according to the phase diagram.[38]

Photoemission experiments were carried out using a monochromatized Al $K\alpha$ source at a photon energy of 1486.6 eV (instrumental resolution approximately 0.6 eV) in a small-spot-size Surface Science XPS instrument at a base pressure of 3×10^{-9} torr. Foils were cleaned by mildly energetic (500 eV) Ar^+ ions *in situ* prior to the measurements.

X-ray absorption experiments were carried out on beamline X-11A of the x-ray ring (2.5 GeV) at the National Synchrotron Light Source. For the energy regions examined, a Si(111) double-crystal monochromator was employed. The foils prepared were of the order of one absorption length in thickness (with negligible thickness effects at the Au L_3 edge), thereby allowing the experiment to be carried out in the transmission mode with N_2 ionization chambers being used as detectors for the I_0 and I flux.

III. RESULTS

A. XPS core-level and valence-band spectra

In a previous work,[5] we have focused on the Cu_3Au order-disorder system in evaluating locally sensitive parameters such as Au Mössbauer isomer shifts, Au $4f$ core-level shifts, Au $L_{2,3}$-edge XANES, and Cu K-edge XANES. This has been expanded here to include a series of alloys with different compositions, and we have also looked at the Cu $2p$ core-level shifts, alloy d-band widths, and "apparent" Au $5d_{5/2}$-$5d_{3/2}$ splitting.

In this section we will report on the results of the photoemission experiments. In this case we have determined the positions of the Au $4f_{7/2}$, Au $4f_{5/2}$, and Cu $2p_{3/2}$ emission levels for pure Au and alloys of increasing Cu concentration to pure Cu. We have also determined the corresponding apparent (quasi) Au $5d$ spin-orbit splitting (assuming a localized model) and alloy d-band widths (d-band widths were determined by measuring the immediate onset of both edges of the band as shown in Fig. 2). These results are given in Table I.

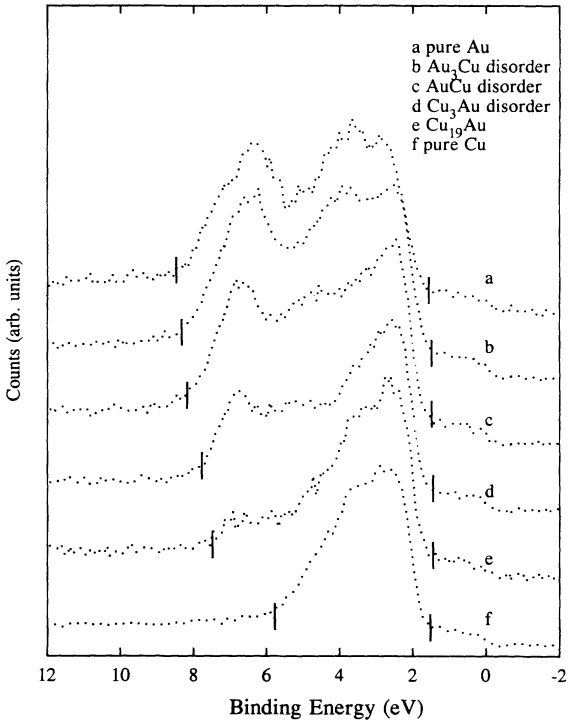

FIG. 2. Representative valence-band XPS spectra of the disordered Au-Cu series and pure Au and Cu using a monochromatized Al $K\alpha$ source. The bold lines indicate the positions taken for measurement of the onset of the bands. The intensities have been normalized to the height of the band just below the Fermi level (approximately 0–1.5 eV).

Focusing on the Au $4f$ peaks, it is noted that there is a shift to higher binding energies as the Cu concentration is increased. The Cu $2p_{3/2}$ peak also shifts to higher binding energy as the Cu concentration increases. Representative spectra are shown in Figs. 3 and 4, respectively. The alloy d band narrows, relative to pure Au, with

TABLE I. XPS-derived parameters (in eV).[a]

Compound	Au $4f_{7/2}$ (±0.05 eV)	Au $4f_{5/2}$ (±0.05 eV)	Cu $2p_{3/2}$ (±0.05 eV)	Alloy d-band width (±0.1 eV)	"Au $5d$" d-band splitting (±0.1 eV)
Au	83.94	87.62		6.44	2.75
Au_3Cu disorder	84.00	87.67	932.11	6.38	2.6
Au_3Cu order	84.00	87.63	932.27	6.32	2.6
AuCu disorder	84.19	87.87	932.26	6.19	2.2
AuCu order	84.25	87.90	932.38	6.19	2.2
Cu_3Au disorder	84.20	87.86	932.33	6.05	1.6
Cu_3Au order	84.31	87.98	932.31	6.05	1.6
$Cu_{0.875}Au_{0.125}$	84.37	88.06	932.37	5.94	1.55
$Cu_{0.95}Au_{0.05}$	84.41	88.10	932.44	5.63	1.5
Cu			932.53	4.50	

[a]Peaks fitted with a polynomial background and a 60% Gaussian–40% Lorentzian line shape.

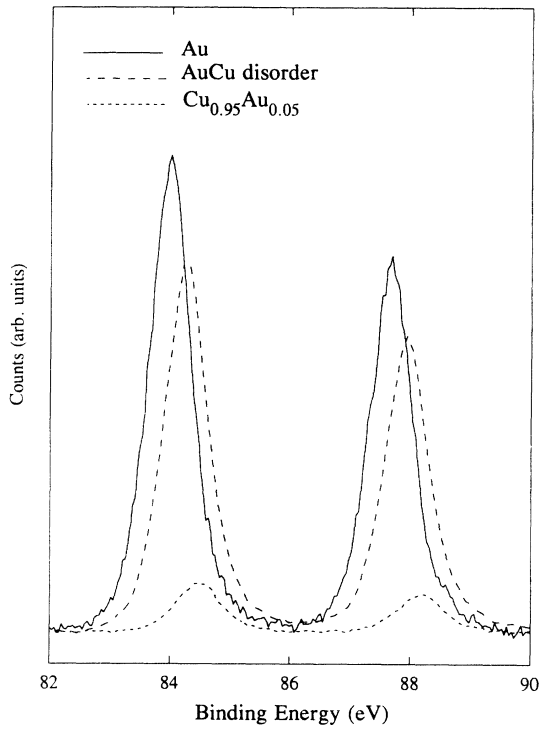

FIG. 3. Representative Au $4f$ XPS spectra of pure Au and Au-Cu alloys using a monochromatized Al $K\alpha$ source.

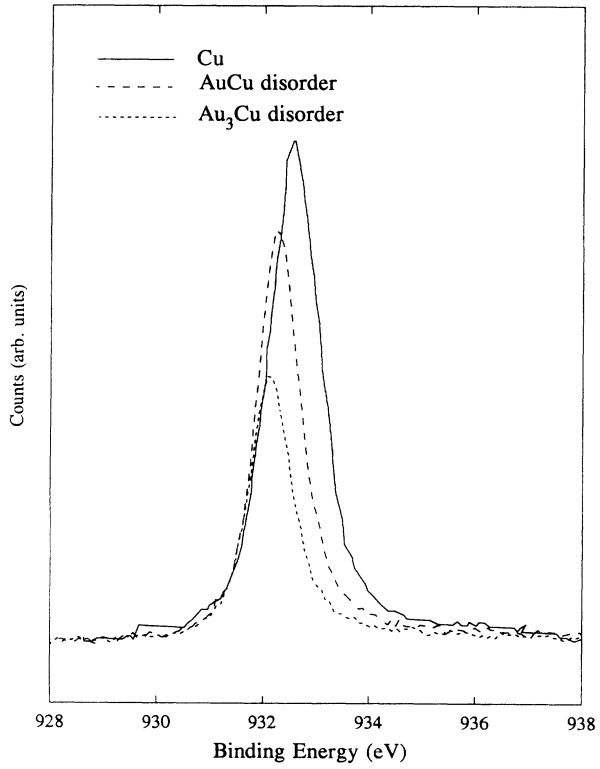

FIG. 4. Representative Cu $2p_{3/2}$ XPS spectrum of pure Cu and Au-Cu alloys using a monochromatized Al $K\alpha$ source [full width at half maximum (FWHM) is 1.09, 1.06, and 1.02 eV for Cu, AuCu, and Au_3Cu, respectively].

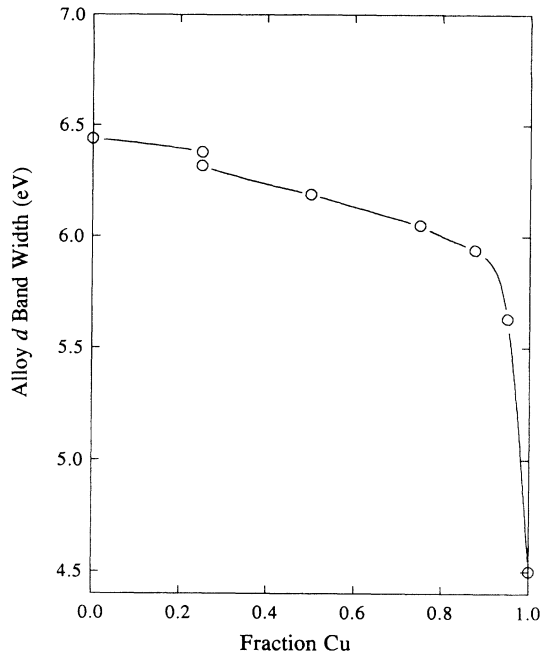

FIG. 5. Experimental alloy d-band width as measured from XPS valence-band spectra (Fig. 2). The uncertainty is ± 0.1 eV.

values between those of the pure constituents (Fig. 2). The experimental d-band width varies slowly and linearly in the high-Au-concentration regime, but reduces drastically once lower Au concentrations (on the order of 10%) are reached (Fig. 5). There is a corresponding shift in the

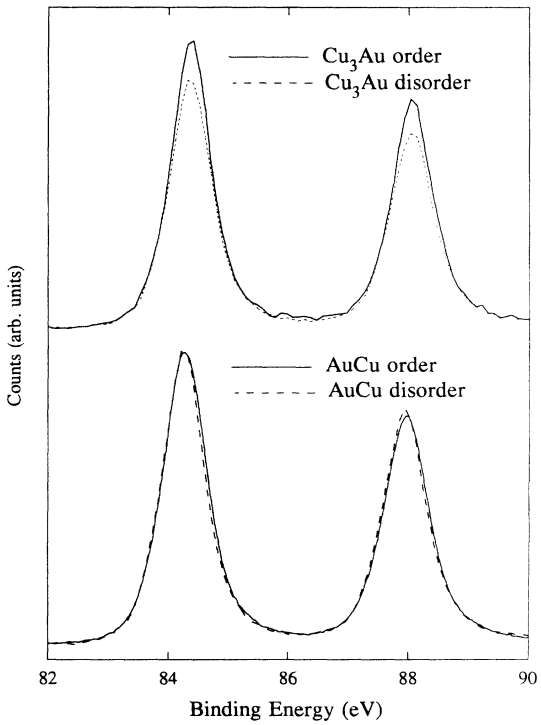

FIG. 6. Au $4f$ XPS spectrum using a monochromatized Al $K\alpha$ source of (a) Cu_3Au order-disorder alloys and (b) AuCu order-disorder alloys.

"Au" contribution of the alloy d band in which the Au $5d_{3/2}$ band remains largely unaffected, but in which the Au $5d_{5/2}$ band shifts away from the Fermi level and the Cu $3d$ band. The "Cu" contribution has narrowed and the centroid shifted toward the Fermi level. A recent high-resolution photon-energy-dependent cross-section study, taking advantage of the Au $5d$ Copper minimum, on Cu_3Au indeed shows, not only the separate contributions of Au and Cu to the alloy d band, but also the shifts of the Au $5d_{5/2}$ band away from and the Cu $3d$ band toward the Fermi level.[29] The atomic terms $d_{5/2}$ and $d_{3/2}$ are merely used for the bands as a simple notation to indicate the origin of the bands. The splitting and width of the bands arise from the interplay of an atomic spin-orbit term and a band formation term.

In the valence-band photoemission data, we find no significant difference between the disordered and corresponding ordered compounds in terms of d-band widths and splittings at our experimental resolution ($\sim$0.6 eV). The core-level shifts, however, show a movement to higher binding energies for the ordered samples (Fig. 6) relative to their disordered phase.

B. XANES spectra

XANES experiments were completed at the Au $L_{2,3}$ (mainly $2p \rightarrow d$ dipole transitions) and Cu K ($1s \rightarrow p$ dipole transitions) edges to determine changes in the density of unoccupied states above the Fermi level upon alloy formation. Representative spectra are given in Figs. 7 and 8, and a summary of the parameters investigated is given in Table II. Relative to pure Au, all of the alloys have noticeable sharp absorption features, often called white lines, at the Au $L_{2,3}$ edges just above threshold. There is an increase in the white-line intensity as the Cu concentration is increased. The spectra also exhibit a

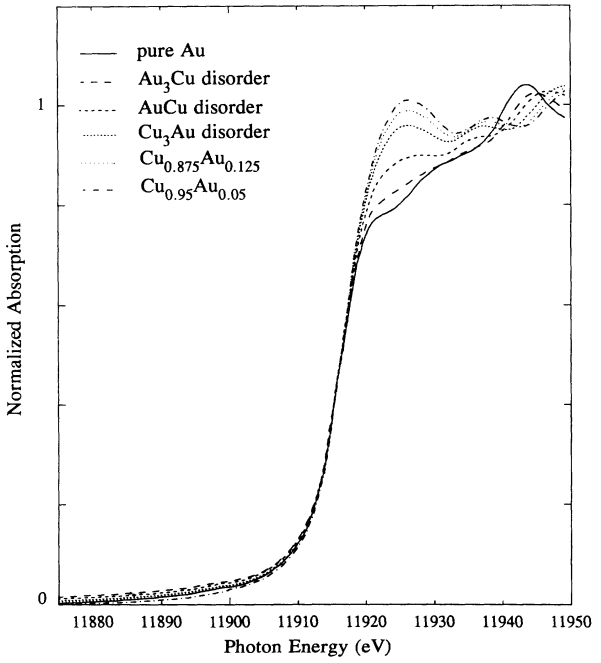

FIG. 7. Representative Au L_3-edge XANES spectra of pure Au and Au-Cu disorder series. The spectra have been calibrated by simulating an arctangent function to imitate the step. The spectra were then lined up at the halfway rise to the step. The portion of the spectrum from which the pure Au spectrum was subtracted begins at the calibration point and extends to $\sim$15 eV above for each alloy.

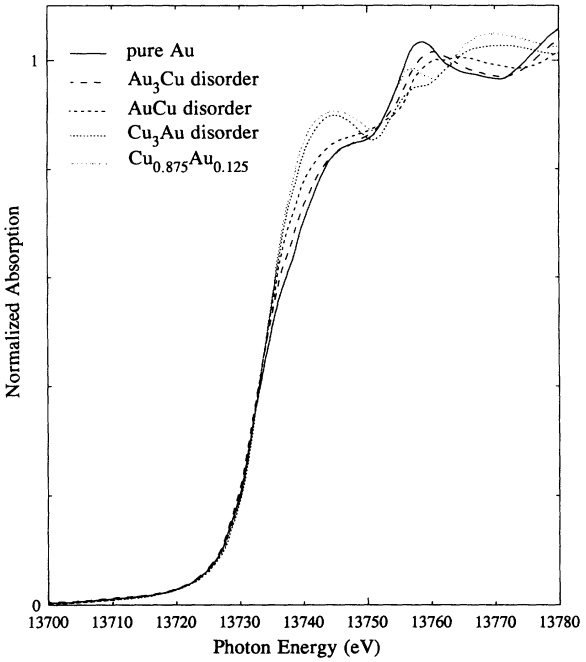

FIG. 8. Representative Au L_2-edge XANES spectra of pure Au and Au-Cu disorder series. The spectra were calibrated and the subtractions performed as described in Fig. 7.

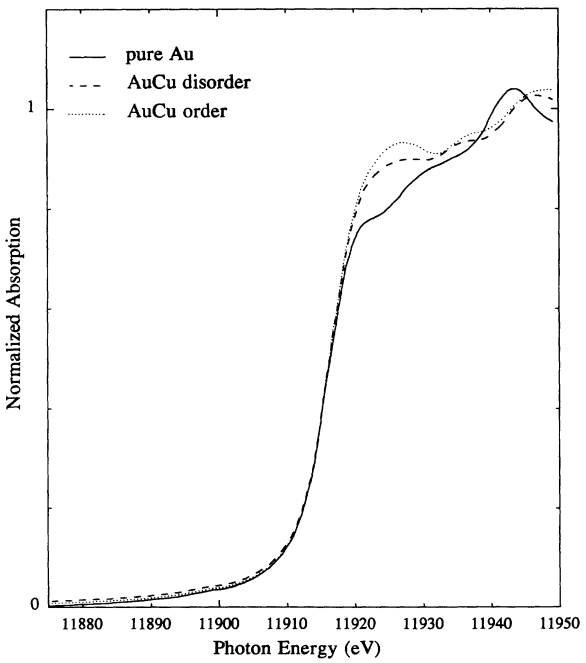

FIG. 9. Au L_3-edge XANES spectra of pure Au and AuCu order-disorder alloys showing the difference in the areas as compared to pure Au for the two alloys. The spectra were calibrated and the subtractions performed as previously described.

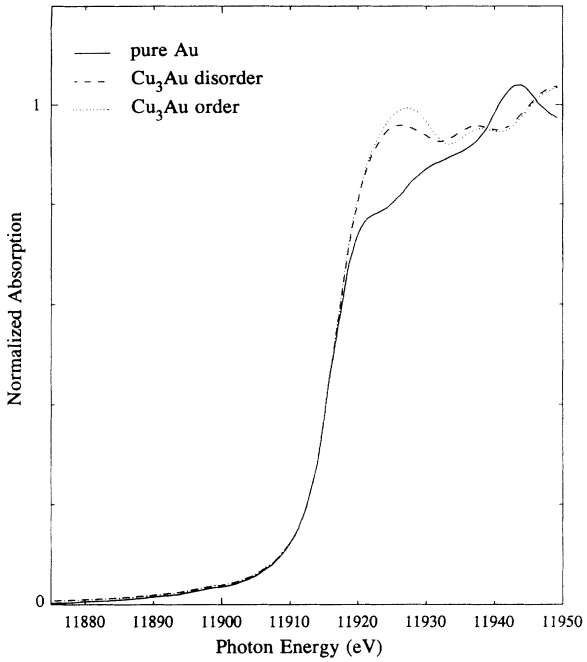

FIG. 10. Au L_3-edge XANES spectra of pure Au and Cu_3Au order-disorder alloys again showing the difference in the areas as compared to pure Au for the two alloys. The spectra were calibrated and the subtractions performed as previously described.

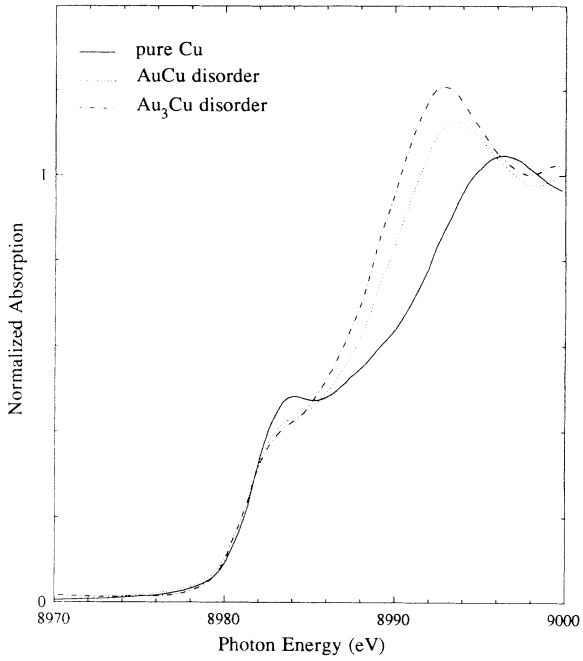

FIG. 11. Representative Cu K-edge XANES spectra of pure Cu and Au-Cu alloys. The same calibration was performed as previously described. We note the small feature on the rising edge.

larger white-line intensity for the ordered samples as compared to their respective disordered counterparts (Figs. 9 and 10).

The Cu K-edge XANES has also been qualitatively analyzed and representative spectra are given in Fig. 11. The small but clearly noticeable pre-edge feature at the absorption edge is attributed to a $1s \rightarrow d$ transition, usually forbidden by dipole selection rules, but from hybridization due to solid formation, the Cu d band contains $l=1$ character and therefore the matrix element is not zero.[39] We note the largest area under this feature for pure Cu, which decreases with increasing Au concentration. Recently completed Cu $L_{2,3}$-edge studies have also shown qualitatively a decrease in the white-line area as the Au concentration is increased.[40] There are also differences associated with disordered and ordered samples. The ordered samples exhibit large decreases in area relative to pure Cu.

IV. ANALYSIS AND DISCUSSION

A. Estimation of Au 5d-hole counts in Au-Cu alloys from XPS and Mössbauer results: The charge compensation model

The apparent opposite trends of XPS Au 4f binding energy and Mössbauer isomer shifts (Tables I and III) with respect to electronegativity difference and dilution between Au and Cu are in accord with the observations of bimetallic Au systems generally.[4-11]

TABLE II. Relevant parameters derived from Au $L_{2,3}$ XANES analysis.

Compound	White-line area (10^4 cm^{-1} eV)[a]		Unoccupied 5d counts[b]					
	ΔA_3	ΔA_2	$\Delta h_{5/2}$	$\Delta h_{3/2}$	Δh_t	h_t[c]	$\Delta h_{5/2}/\Delta h_{3/2}$	$h_{5/2}/h_{3/2}$
Au_3Cu disorder	0.05	0.01	0.019	0.004	0.022	0.423	0.350	2.48
Au_3Cu order	0.05	0.02	0.018	0.006	0.024	0.425	2.33	2.43
AuCu disorder	0.16	0.04	0.060	0.017	0.076	0.477	2.55	2.54
AuCu order	0.27	0.05	0.099	0.017	0.116	0.517	4.22	2.83
Cu_3Au disorder	0.28	0.08	0.104	0.029	0.133	0.534	2.60	2.63
Cu_3Au order	0.34	0.10	0.125	0.036	0.161	0.562	2.53	2.65
$Cu_{0.875}Au_{0.125}$	0.35	0.12	0.126	0.045	0.171	0.572	2.00	2.51
$Cu_{0.95}Au_{0.05}$	0.39	0.10	0.144	0.034	0.178	0.579	2.82	2.81

[a]Edge jump values from Ref. 44.
[b]$C_0=0.096\,05$, $R_{5d}^{2p}=3.103\times10^{-11}$ cm, $N_0=5.922\times10^{22}$ atoms cm^{-3}, and $E_2=13.733$ keV were used in the calculation relative to pure Au; total error in area determination is $\sim 10\%$.

We first analyze the XPS core-level binding energy shifts within the single-particle framework. According to the charge compensation model, we would expect the Au $4f$ core levels to shift to higher binding energies with increasing Cu concentration, indicating a loss of d charge at the Au site. The loss of d charge is the dominant term. It leads to a higher effective Coulombic potential for the remaining electrons, giving a shift to higher binding energies, even though there is an overcompensation of (less effective) conduction charge as required by electronegativity considerations. The results given in Table I do indeed show a shift to higher binding energies throughout the Au-Cu series. These results indicate that the smaller the number of like nearest neighbors, the higher the binding energy shift. The corollary of the shifting of the Au $4f$ peaks is the expected shifting of the Cu core levels. The Cu $2p_{3/2}$ levels investigated shift to lower binding energies with increasing Au concentration. This indicates that Cu is gaining d and/or non-d charge. We will briefly examine the results of the absorption at the Cu K edge. The Cu K-edge XANES clearly reveals a decrease in the density of unoccupied d states, upon alloying, with a decreased area in the feature at the absorption edge. This indicates an increase of d charge at the Cu site. With the loss of d electrons (as exhibited by the increase in white-line intensity at the Au $L_{2,3}$ edges), the gain of conduction electrons (as exhibited by positive Mössbauer shifts), and the fact that Au must gain overall charge (as required by electronegativity arguments) at the Au site, it eliminates the possibility of the shifts being due to a gain of s-p-like conduction charge at the Cu site. The differences found in the ordered and disordered samples will be discussed later.

By using Au $4f_{7/2}$ binding energy shifts (ΔE_{Au}) and the corresponding conduction (primarily $6s$) charge flow (Δn_c) derived from Mössbauer isomer shifts, the $5d$ count depletion at the Au site (Δn_d) and the net charge flow (δ) can be obtained. The procedure used for determining Δn_d has been described previously[5,6] and will only be outlined here. Simply stated, the shift in the Au $4f$ core levels is related to changes in the one-electron energy and the position of the Fermi level. The former is related to the Coulombic interaction of the core levels with both the valence $5d$ electron and the $6s$ conduction electron at the Au site in an alloy and the net charge transfer in the normalized atom scheme[5] (within the Wigner-Seitz volume of the Au atom), while the latter is related to work function changes. If we neglect any difference in final-state screening effects (a reasonable assumption for a metallic system), the binding energy shifts can be expressed as[5]

$$\begin{aligned}\Delta E_{\mathrm{alloy-Au}} = &-(\Phi_{\mathrm{alloy}}-\Phi_{\mathrm{Au}}) \\ &-\Delta n_c[F^0(4f,c)-F^0(4f,5d)] \\ &-\delta[F^0(4f,5d)-F(\mathrm{latt})] \\ &+\left[\frac{dE}{dV}\Delta V\right]_{\mathrm{Au}} . \end{aligned} \tag{1}$$

The Φ's are the work functions, which, to the first approximation, represent the Fermi-level shift relative to the vacuum upon alloying (values used for the various alloys were estimated by a linear scale between the value of pure Au and pure Cu dependent on concentration only). The F^0 terms are the Coulomb integrals associated with the removal of a conduction or $5d$ electron and are estimated to account for the relaxation of the system in question. F(latt) is a Madelung-like potential energy associated with charge transfer in and out of the Wigner-Seitz volume and is evaluated by placing a charge at the Wigner-Seitz radius. The overall charge transfer is given by $\delta=\Delta n_c+\Delta n_d$. The last term is the shift in binding energy associated with the change in the volume of the Au site upon alloying. The change, though, is small as shown in the case of $AuCu_3$ and other Au-Cu alloys. For example, the ratio of the volume of Cu_3Au and the sum of the constituent volumes $[V_{\mathrm{Cu_3Au}}/(V_{\mathrm{Au}}+3V_{\mathrm{Cu}})]$ $\simeq 1.006$, which is a slight positive deviation (0.6%) from Vegard's law. For this reason we ignore the last term in our calculations.

The results of the analysis based on Eq. (1) and the various parameters used are given in Table III. As we increase the Cu concentration, there is an increase in the loss of d charge and also an associated higher loss of d charge for the ordered species. The loss of d charge varies from 0.05 for Au_3Cu to 0.21 for $Cu_{0.95}Au_{0.05}$, and the corresponding gain in s charge is 0.08–0.32. There is also a corresponding increase in the overall transfer of charge to the Au site, in accordance with electronegativity arguments. The ratio of $(\Delta n_d/\Delta n_c)$, however, remains

TABLE III. Relevant experimental and derived parameters (relative to pure Au).

Compound	ΔE (Au $4f_{7/2}$)	$\Delta\phi$	Δn_c[a]	Δn_d[b]	δ[b]	$\Delta n_d/\Delta n_c$
Au_3Cu	0.06	−0.10	0.083	−0.045	0.038	−0.54
Au_3Cu (annealed)	0.06	−0.10	0.083	−0.045	0.038	−0.54
AuCu	0.25	−0.21	0.183	−0.117	0.066	−0.64
AuCu (annealed)	0.31	−0.21	0.187	−0.127	0.060	−0.68
$AuCu_3$ (disorder)	0.24	−0.31	0.276	−0.159	0.117	−0.58
$AuCu_3$ (order)	0.37	−0.31	0.291	−0.185	0.106	−0.64
$AuCu_7$	0.43	−0.36	0.315	−0.201	0.114	−0.64
$AuCu_{19}$	0.47	−0.39	0.324	−0.208	0.116	−0.64

[a]Derived from Mössbauer data (Δn_c = isomer shift $\times 0.0833$).
[b]Calculated according to Eq. (1) with parameters $F^0(4f,c)-F^0(4f,5d)=-3.0$ eV and $F^0(4f,c)-F(\mathrm{latt})=7.7\pm1$ eV.

essentially a constant, in accordance with previous observations.[7]

B. Charge redistribution, valence-band spectra, and dilution

We next investigate the effect of charge redistribution on the XPS valence-band behavior. Assuming that the valence band features primarily separated d bands, a comparison of the change in the splitting of the "Au" portion of the alloy d band, $\Delta_{\text{apparent}}(\text{alloy})$, versus an empirically derived relationship[41]

$$\Delta_{\text{apparent}}(\text{alloy})=[(\Delta_{\text{atomic}})^2+(\Delta_{\text{electronic}})^2]^{1/2} \quad (2)$$

can be made (Fig. 12). The apparent alloy d-band splitting, below 3 eV relative to the Fermi level, is assumed to be dominated by the Au d bands and is related to the convolution of two terms: an atomic Au $5d$ spin-orbit splitting term of 1.5 eV and an intrinsic band term. Using experimental values of pure Au (1.5 eV for the atomic splitting and the experimental value of 2.75 eV for the apparent splitting), the electronic band term is estimated to be 2.3 eV. For the series of alloys, Δ_{elec} is determined by using the pure Au value and the reduction of like nearest neighbors in the disordered alloy with the following relationship:[42,43]

$$\frac{\Delta_{\text{elec}}(\text{pure})}{\Delta_{\text{elec}}(\text{alloy})}=\frac{[N(\text{pure})]^{1/2}}{[N(\text{alloy})]^{1/2}} . \quad (3)$$

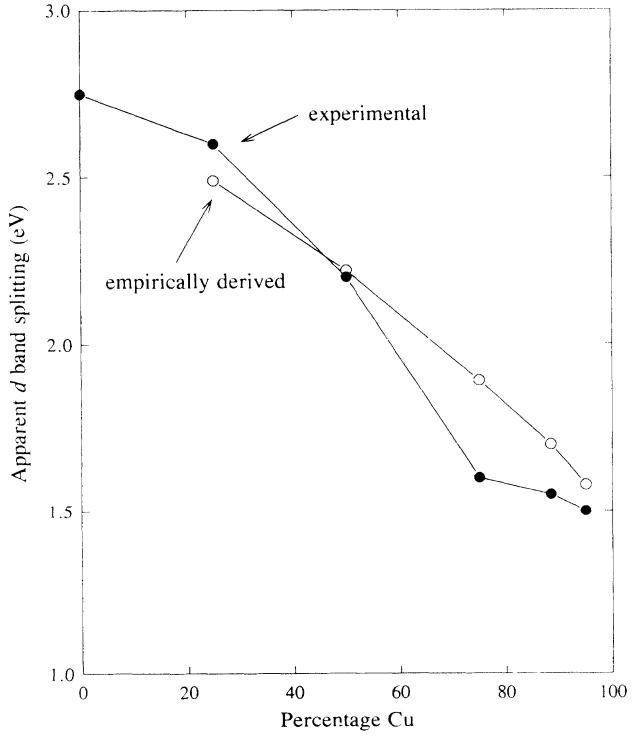

FIG. 12. Comparison of the experimental "Au 5d"-band apparent spin-orbit splitting of the Au-Cu disorder series with an empirically derived relation.

This model assumes that little or no Au-Cu d-band mixing occurs and that the changes in the alloy d-band widths are a function of dilution only (i.e., dominated by the Au-Au interaction). For systems in which order and disorder states exist, the nearest-neighbor values for the disorder state (statistical probability) only were used. To properly evaluate the ordered states, we would have to include second-order effects, i.e., the distribution in the second shell. In examining Fig. 12, we see that the Au portion of the experimental d-band splitting correlates with the dilution model at low Cu concentrations, but deviates as the Cu concentration is increased. A maximum deviation is observed for Cu_3Au. The experimental values of the splitting have a large error due to the low resolution of the spectra and the fact that at low Au concentrations the emissions are very weak (see Fig. 4).

The experimental alloy d-band width decreases linearly in the low-Cu-concentration regime, but falls off drastically once higher Cu concentrations are reached ($\sim 90\%$, Fig. 5). Again, there is a larger error in determining the width at high Cu concentrations since Au is so dilute that the emission is quite weak and the onset of the band is harder to determine. Assuming that the "Au" and "Cu" components of the alloy d band are still valid, we find, from Fig. 4, that there is a reduction in the width of the respective "Au" and "Cu" components as we reach higher concentrations of unlike nearest neighbors (the "Au" width reduces going down Fig. 2, while the "Cu" width reduces going up Fig. 2). In Ref. 29 we have completed photon-dependent photoemission studies on the order-disorder Cu_3Au system. At 160 eV the cross section of the Au $5d$ band is at a minimum and it is clear from our data that the Cu contribution to the alloy d band is highly localized from 1.5 to 4.5 eV below the Fermi level and has little overlap with the Au contribution. It was also noted that the Cu portion of the alloy band is a lot narrower than that of the pure Cu $3d$ band at 160 eV.

Examination of the centroid shifts of the d-band components lends support to the d-d repulsion model. We observe a large shift of the "Au" centroid away from the Cu centroid and the Fermi level. The largest movement is that of the "Au $5d_{5/2}$" band. Accompanied with this is a smaller shift of the "Cu" centroid towards the Fermi level. This repulsive behavior is typical for the Au-Cu system and has clearly been seen for two-dimensional Au-Cu alloys on Ru(001).[44]

No discernible differences are detectable in the valence-band features between the ordered and disordered Au-Cu alloys. The error in measurement is relatively large (± 0.1 eV) compared to possible changes that are present upon ordering. It can be argued that from the dilution model we would expect the apparent splitting and d-band width to be smaller in the ordered alloys since the ordered alloys have a smaller number of Au nearest neighbors (these features are dominated by Au-Au interactions). However, the ordered alloys do have a larger number of Au next-nearest neighbors, and thereby second-order effects may contribute to maintaining both the d-band width and apparent splitting. High resolution is needed to resolve these small differences.

C. XANES and Au 5*d*-hole count

Correlation of *d*-hole count and XANES white-line intensities dates back to several decades ago when Mott[31] first pointed out that for the L_1 adsorption edge of platinum no white-line intensity is expected or experimentally seen. This is due to the dipole selection rule of $\Delta l=\pm 1$ and $\Delta j=0,\pm 1$, giving a low transition probability (matrix element) for the L_1 core state (*s* character) to the empty *d* states. It was also seen in metallic Pt that there was white-line intensity at the L_3 absorption edge and no appreciable intensity at the L_2 absorption edge. Mott also pointed out that this can be explained by symmetry selection rules arising from spin-orbit coupling and the band structure of Pt. The initial core states for the $L_{2,3}$ edges have $2p_{1/2}$ and $2p_{3/2}$ symmetry, respectively, while the empty states in the *d* shell in Pt metal primarily have a *j* value of 5/2; therefore, only transitions from the $2p_{3/2}$ core states are allowed, giving a white-line intensity at the L_3 absorption edge. For metallic Pt the assumption is made that the spin-orbit coupling has not completely broken down, as shown experimentally by Cauchois and Manescu[32] and by Coster and De Lang.[33] Since then, there have been continuous efforts. For example, Brown, Peirls, and Stern[34] have shown, using a tight-binding approximation for the unoccupied Pt *d* states, that the ratio of $j=\frac{5}{2}$ to $\frac{3}{2}$ in the unoccupied states is about 14 to 1. Mattheiss and Dietz,[30] using relativistic band calculations, obtain a ratio much closer to the experiment. It was also shown qualitatively by Lytle *et al.*[35] that the increase in white-line intensity is proportional to the number of vacancies in the *d* states. In our case we are looking at the $L_{2,3}$ absorption edges of Au. For metallic Au the 5*d* bands are nominally full, but because of hybridization with overlapping *s-p* bands, there are about 0.4 5*d* holes, according to Mattheiss and Dietz,[30] with a $h_{5/2}/h_{3/2}$ ratio of approximately 2.4. This has been confirmed by experiment.[11(a)] From our experimental results, though, we note that there is no sharp white-line intensity in our pure Au samples, while our alloy samples exhibit relatively intense white lines, indicating a greater localization of *d* states as compared to the pure samples.

Using these previous observations, Mansour, Cook, and Sayers[36] have extended the analysis of the white-line areas to include determining hole counts in various Pt systems.

According to this scheme, the total x-ray absorption coefficient is written as

$$\mu=\mu_{\mathrm{Li}}+\mu_0 ,$$

where μ_{Li} is the absorption due to the $2p_{1/2,3/2}$ electrons and μ_0 is the absorption due to all other electrons. In fitting our data, we have used a pre-edge background subtraction to account for the decreasing contribution of the other electrons above the edge.

To separate the contributions to μ_{Li} by unoccupied *d* and *s* states, we have assumed that the *s* states are delocalized above the Fermi level with a transition-matrix element at least one order of magnitude smaller than that for the excitation into empty *d* states and that their contribution can be neglected.[45] By subtracting the absorption spectrum at the $L_{2,3}$ edges of pure Au from that of the alloys, all the parameters derived are then relative to pure Au and therefore the hole counts and changes in the white-line areas are changes due to alloy formation. It should be noted that Au gains *s* charge upon alloying (decreasing *s* count). The fact that the white-line area increases in alloys again supports the fact that the change in *d* counts is primarily responsible for the change in the area under the white line. In lining up the edges for subtraction, we must also take into account the effect of a localized density of unoccupied states at, or very near, the Fermi level. As indicated by Mansour, Cook, and Sayers,[36] a sharp white line at the absorption edge will shift the apparent Fermi level, and for this reason, instead of lining up the inflection points of the edge jumps of our alloy and reference spectra, we have opted for shifting the spectra so that the halfway points of an arctangent simulating the edge jump and ignoring the white line are lined up. Since the difference in the edge threshold (a few tenths of an eV) and the white-line intensities are relatively small, the uncertainty in the analysis is not significant ($<10\%$). [The exception to this is the Au L_2-edge spectra (Fig. 8). Because of the lower signal and possible variant contribution from absorption at the L_3 edge, depending on the alloy, it was impossible to line up the rising edge with calibration at the halfway point. For proper overlap the calibration point is a little below the halfway point.]

The areas thus derived from our experimental data can be expressed as

$$A_2=\int[\mu_{L_2}(\text{alloy})-\mu_{L_2}(\text{Au})]dE , \tag{4a}$$

$$A_3=\int[\mu_{L_3}(\text{alloy})-\mu_{L_3}(\text{Au})]dE . \tag{4b}$$

Following Mattheiss and Dietz[30] and assuming there is no countervailing symmetry arguments, expressions relating the area under the white line (A) to hole counts (Δh, where Δ means with respect to pure Au) are given by

$$A_2=C_0N_0E_2(R_d^{2p_{1/2}})^2(\tfrac{1}{3}\Delta h_{3/2}) , \tag{5a}$$

$$A_3=C_0N_0E_3(R_d^{2p_{3/2}})^2\left[\frac{6\Delta h_{5/2}+\Delta h_{3/2}}{15}\right] , \tag{5b}$$

where $C_0=4\pi^2\alpha/3$ (α is the fine-structure constant), N_0 is the density of Au atoms, $E_{2,3}$ are the absorption edge energies, and the R term is the radial dipole integral. If, in the first approximation, we let the radial dipole-moment integral for the two excitation processes be the same, we can derive the relationship between the change in hole counts, relative to pure Au, to the white-line areas:

$$\Delta h_{5/2}=\frac{1}{2C}\left[5\frac{E_2}{E_3}A_3-A_2\right] , \tag{6a}$$

$$\Delta h_{3/2}=\left[\frac{3A_2}{C}\right] , \tag{6b}$$

where

$$C = C_0 N_0 E_2 (R_d^{2p})^2 .$$

If we use the value of the dipole transition-matrix element for platinum (3.103×10^{-11} cm) (we have shown recently that this is a very good approximation[12]), the Au atomic number density (5.894×10^{22} atoms cm^{-3}), and the L_2-edge energy of 1.373×10^4 eV, we get $C = 7.484 \times 10^4$ eV cm^{-1}. To normalize our data and incorporate the appropriate units, the integrated areas determined from the experiment (from just below the edge to approximately 15 eV above) must now be multiplied by the edge jump absorption coefficient of a Au atom. (The $\Delta\sigma_{2,3}$ are the x-ray absorption cross-section differences above and below the absorption edges and are 105.3 cm^2 g^{-1} for the Au L_3 edge and 50.7 cm^2 g^{-1} for the Au L_2 edge.) From the multiplicity of the initial states, we expect a ratio of 2 to 1 in edge heights, yet experimentally the ratio is found to be 2.2 to 1, and reported in the tables of McMaster *et al.*[46] as 2.1 to 1. The differences can be explained by the fact that we have assumed both transition dipole moments to have the same value. Therefore, to directly compare the derived areas from the L_2 and L_3 spectra, we have scaled the $\Delta\sigma$ values to reflect the experimental ratio.

The calculated areas and hole populations are given in Table II with an accompanying list of the parameters used in the calculations. Figure 13 summarizes the trends shown by the previous calculations. Let us concentrate on the upper panel of Fig. 13 for the moment. As we increase the Cu concentration, that is, as Au becomes more dilute, there is a large increase in the total hole count, which slows as higher concentrations of Cu are reached. The ordered samples consistently have higher hole counts than their disordered counterparts. The total change in hole count relative to pure Au varies from 0.02 for Au_3Cu to 0.18 for $Cu_{0.95}Au_{0.05}$. It can also be seen that there is a larger contribution to the total hole count from the $h_{5/2}$ states than from the $h_{3/2}$ states and that the higher total hole counts for the ordered samples arise directly from increased number of $h_{5/2}$ states.

D. Correlation of XANES Au *d* holes (Δh_t) and Mössbauer isomer shifts

Using the change in total hole count, Δh_t, derived from XANES analysis and Mössbauer isomer shifts, we can establish the relationship between 6*s* gain and 5*d* depletion at the Au site. One of the important uses of Mössbauer results is to correlate the isomer shift (relative to pure Au) with changes in electronic structure. Previous studies have assumed that the isomer shift (IS) is related only to the change in 6*s* count at the Au nucleus using the relationship

$$\mathrm{IS} = a\,\Delta n_s , \tag{7a}$$

where a represents a value of 8 mm s^{-1} for the complete transfer of a 6*s* electron.[47,48] This relationship could not explain some experimental results, such as for the metallic $AuAl_2$ system, which showed an isomer shift of approximately 7 mm s^{-1}. It is unreasonable to assume that Au would gain approximately 0.9 electrons in a metallic system which must maintain electroneutrality. It was suggested that a value of 12 mm s^{-1} is more appropriate for metallic systems and that there is a significant contribution from Au 5*d* depletion.[7,49,50] The following analysis will use the Au 5*d*-hole count derived by XANES analysis as an independent verification of the contribution of the Au 5*d*-charge transfer to Mössbauer isomer shifts and provide further verification of the charge compensation model.

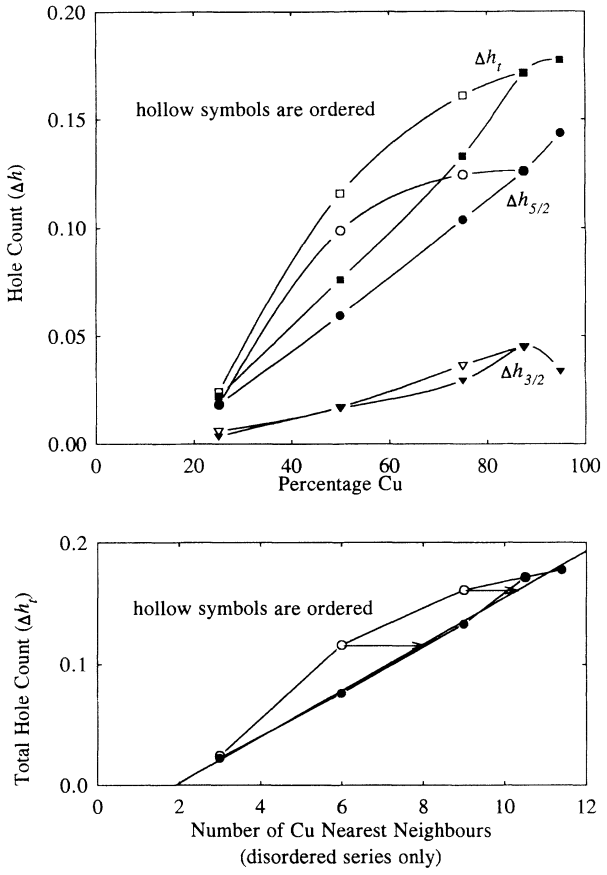

FIG. 13. Comparison of the XANES-derived hole counts (Δh_t, $\Delta h_{5/2}$, and $\Delta h_{3/2}$) with bulk Cu concentration. The bottom spectrum gives a line of best fit for the Au-Cu disorder series. The correlation factor is 0.998 with an intercept of -0.036.

Taking into account all possible contributions, the ^{197}Au isomer shift or change in contact density at the nucleus, upon alloy formation, can be empirically expressed as

$$\mathrm{IS} \propto a\,\Delta n_s + b\,\Delta n_d + d\,\Delta n_p , \tag{7b}$$

where Δn_s is the change in the number of 6*s* electrons, Δn_d is the change in the number of *d* electrons and is included since the effective potential experienced by *s* electrons varies with the change in the number of *d* electrons which have a high screening ability, and Δn_p is the charge in the number of *p* electrons. Δn_p can be ignored because of their modest contribution in hybridization and

their ambivalent contribution in $p_{1/2}$ contact density and screening and the fact that overall their screening ability is much smaller than for d electrons ($\Delta n_p \ll \Delta n_s$). The isomer shift and Δn_c ($\sim \Delta n_s$) are related by the empirical equation $\Delta n_c = 0.0833 \times \mathrm{IS}$ for intermetallic systems assuming a conversion factor of 12 mm s^{-1}.[42,47] In Fig. 14 we have plotted the isomer shift versus the d-hole count and observe a linear relationship. The line does not go through zero, but as will be explained shortly, the XANES-derived d-hole counts are most likely slightly underestimated and have a larger error at low Cu concentrations (low hole counts). If the d-hole values are underestimated by a constant 10–15 %, then the correlation line will go through zero and with a larger error for the low values the underestimation may be only 10%. By comparison of the values obtained for Δn_d and the independently arrived values for d-hole counts, Δh_t (Fig. 15), we are able to substitute the d-hole values for Δn_d ($\Delta n_d \sim -\Delta h_t$). Since both Δn_d and Δn_c vary linearly with the isomer shift, we can set the ratio of the two to be a constant, and to maintain electroneutrality that is required for metallic systems, we note that Δ and especially δ must be small, as is seen in our case with values no higher than 0.3 and 0.1, respectively. Therefore, if we let $\Delta n_d / \Delta n_c = c$ and substitute for the IS, we can express the IS in terms of Δn_c:

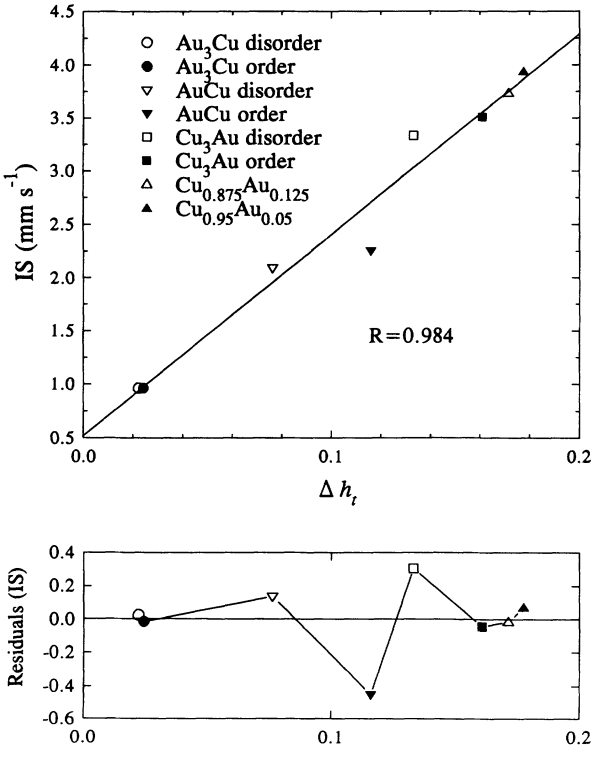

FIG. 14. Comparison of Mössbauer isomer shifts with the XANES-derived hole count (Δh_t) for the Au-Cu alloy series. The line of best fit has a correlation factor of 0.984 with a slope of 18.9 and an intercept of 0.52. The bottom spectrum is a representation of the residuals.

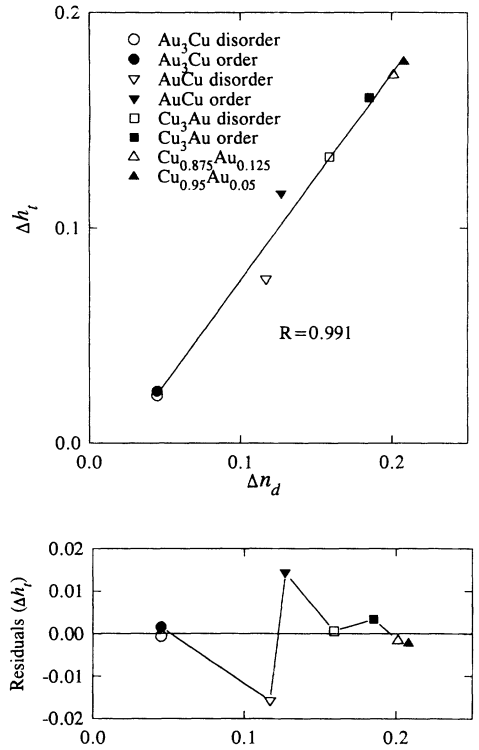

FIG. 15. Comparison of the XANES-derived hole count (Δh_t) with the d-charge transfer derived from the Mössbauer XPS data for the Au-Cu alloy series. The line of best fit has a correlation factor of 0.991 with and intercept of -0.021. The bottom spectrum is a representation of the residuals.

$$\mathrm{IS} = a\Delta n_c + (cb)\Delta n_c = \Delta n_c (a + cb) , \tag{7c}$$

by $\Delta n_c = 0.0833 \times \mathrm{IS}$; therefore,

$$a + cb = 12.00 . \tag{7d}$$

We can also substitute for Δn_c, into the original equation, where we can express the IS in terms of Δn_d:

$$\mathrm{IS} = \Delta n_d \left[\frac{a}{c} + b \right] . \tag{8a}$$

From the plot of the IS versus Δh_t, the slope was determined to be 18.9; therefore,

$$\frac{(a + cb)}{c} = -18.9 . \tag{8b}$$

Dividing Eq. (7c) by (8b), we get

$$c = \frac{\Delta n_d}{\Delta n_c} = -0.63 . \tag{9}$$

Thus, for the Au-Cu system, we have determined the ratio of d-charge versus s-conduction-charge transfer to be -0.63. This value is in good agreement with the $\Delta n_d / \Delta n_c$ ratios given in Table III and is also consistent with values previously seen for a variety of Au intermetallics.[7] Since this result has been independently arrived at through analysis using Mössbauer and XANES results, it further confirms the charge compensation model.

E. Comparison of Au 5*d*-hole counts derived from XPS Mössbauer and XANES analysis and comparison with valence-band features

It is interesting to compare the change in *d* counts derived from these two methods. Both methods give the same trend for the hole values with the numbers derived from the XANES analysis consistently giving slightly lower values (Tables II and III and Fig. 15). For the estimation of the *d*-charge transfer, as determined by core-level shifts and Mössbauer isomer shifts, there is uncertainty in the Coulomb integral values (see Table III) and the work functions; and it must also be taken into account that the XPS core-level shifts may also introduce uncertainty since XPS is sensitive to contributions from the surface layer in terms of surface segregation. Scanning Auger studies of polycrystalline Cu_3Au samples clearly show different surface ratios of Au and Cu for the ordered and disordered species.[51] Also, XANES spectra clearly show a large difference between the two AuCu samples, but this is not reflected as clearly by the experimental Au 4*f* core-level shifts. Yet when examining Fig. 15, it is clear that there is a strong correlation between the XPS-Mössbauer-derived hole counts with the bulk values derived from the XANES analysis. It can be understood, however, that even though the XPS core-level shifts may be slightly skewed by surface segregation, these shifts are small as compared to work function and Coulomb integral values as the latter are dominant terms (see values in Table III). The values determined by the XANES analysis are likely to be slightly underestimated because of uncertainty in the transition-matrix element and because of omission of some of the dispersed unoccupied *d* states above the Fermi level by limiting the analysis to 15 eV above the edge. In a recent report,[12] the area of the difference spectrum of pure Au L_3 and L_2 edges was determined. This shows the distribution of unoccupied states of *d* character which appears concentrated within about 20 eV above the edge. We have limited the analysis to 15 eV to include lifetime contributions [$\sim$8 eV for the L_3 edge of Au (Ref. 52)], but to avoid including features attributed to multiple-scattering effects, and therefore have not included a portion of the tail of the distribution. This, of course, assumes that the alloy *d* states have a similar distribution and that upon alloying the centroid of the distribution does not shift higher by more than a few eV (our data do indicate a more localized distribution of empty *d* states from the relative intense white line as compared to the pure Au sample). This underestimation and the larger errors in the small hole counts could easily compensate for the correlation of the two methods to go through zero.

Overall, the XANES results independently confirm the charge compensation model. However, it is expected that the XANES analysis will give closer to true values since this analysis is derived from first principles and contains fewer assumptions, while the formula based on Mössbauer and Au 4*f* binding energy shifts for elucidating *d*-charge transfer has large uncertainties in all its parameters (see Table III).

In addition, XANES results show that not only is the total hole count important, but also the ratio of the $d_{5/2}/d_{3/2}$ unoccupied densities of states and the ratio of these states to the total hole count change upon alloying. The unoccupied *d* states have a nonstatistical ratio considerably higher than the statistical ratio. For example, the $\Delta h_{5/2}/\Delta h_{3/2}$ ratio (Table II) varies between 2 and 4 and is much higher than the statistical value of 1.5. Also, if we include the calculated distribution of *d* holes in pure Au,[30] we get a $h_{5/2}/h_{3/2}$ ratio that varies between 2.4 and 2.8. The answer lies in taking a look at the alloy valence band from a chemical perspective. The valence band for all the alloys shows that the $5d_{5/2}$ band lies about 2.3–3.0 eV closer to the Fermi level than the $5d_{3/2}$ band as a result of the apparent *d* band splitting. The Au $5d_{5/2}$ band also overlaps strongly with the Cu 3*d* band. The strongest interaction and mixing of states involve those overlapping in energy and closest to the Fermi level. In this case this involves the Au $5d_{5/2}$ and the Cu 3*d* electrons, and for this reason we may expect a proportionally larger loss of Au $5d_{5/2}$ electrons to the Cu site and thereby a nonstatistical ratio of *d*-hole states. This change in *d*-hole count is less evident in the occupied density of Au 5*d* states since we are talking about, in the most extreme case, the loss of approximately 0.2 electrons from a band originating from about 10 electrons per atom. This increased chemical activity of the Au $5d_{5/2}$ over the Au $5d_{3/2}$ band has also been shown for the surface alloying of Au and Cu on Ru(001) in which the $5d_{5/2}$ states shift away from the Fermi level upon alloy-

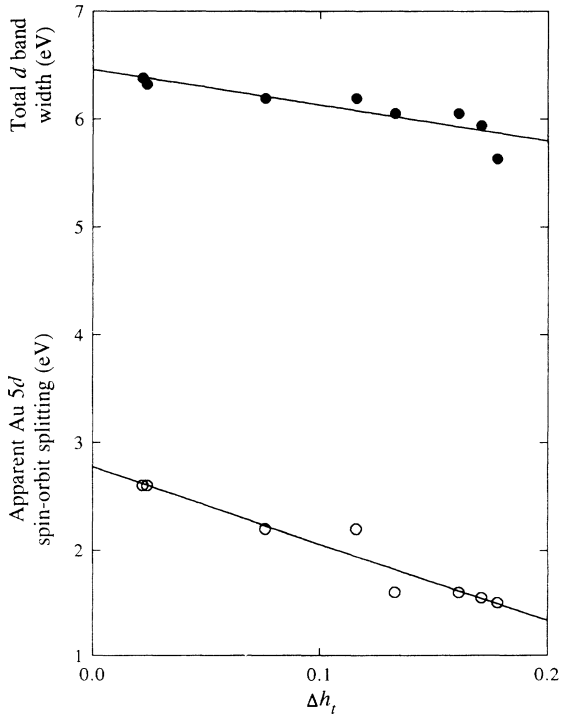

FIG. 16. Comparison of the XANES-derived hole count (Δh_t) with the experimental alloy *d*-band width (top) and apparent "Au" 5*d* spin-orbit splitting (bottom) for the Au-Cu alloy series. Both comparisons have a line of best fit; the top has a correlation factor of 0.874 with an intercept of 6.46; the bottom has a correlation factor of 0.962 with an intercept of 2.78.

ing, while the $5d_{3/2}$ states remain fixed.[44] The Au-Cu interaction can also be viewed as the disruption of the Au-Au interaction.

It is also interesting to compare the XANES-derived d-hole counts with other parameters derived from the XPS analysis, namely, alloy d-band width and apparent d-band splitting (Fig. 16). In previous analysis the d-band width and splitting did not correlate that well with compositional changes (see Figs. 5 and 12). Yet when these parameters are plotted against the d-hole count, there is a strong linear dependence especially for the disordered species. A line of best fit was calculated and extrapolated to Δh_t equal to zero (corresponds to pure Au). The calculated values of the d-band width and splitting for pure Au compare favorably with the experimental values, 6.46 versus 6.44 eV and 2.78 versus 2.75 eV, respectively. This relationship shows the interplay between d-charge transfer and the dilution model with which the "Au" $5d$ splitting and alloy d-band width changes are rationalized.

F. Charge redistribution and the local structure at the Au site

To examine these results more quantitatively, the structures of these alloys become important as does the interatomic distance. Leaving aside the ordered species, the disordered alloys exhibit changes in average nearest-neighbor distribution and distances with changing concentration. In the disordered fcc structure of Cu_3Au, Au has an average of nine Cu neighbors with a lattice parameter of 3.754 Å.[53] (This reference was used as a guide in determining the approximate lattice spacing as their preparation of the alloys was very similar to ours.) In the disordered fcc structure of AuCu, Au has an average of six Cu neighbors with a lattice parameter of 3.874 Å.[53] In the disordered fcc structure of Au_3Cu, Au has an average of three Cu neighbors with a lattice parameter of 3.983 Å.[53] In examining Fig. 13 it is clear that a linear relationship exists between the XANES-derived hole counts and the number of nearest Cu neighbors (reflected by the percentage of Cu) for the disordered species and the dilute Au species. This relationship has been suggested previously.[24] This is evident in the total hole counts and especially the contribution from the $d_{5/2}$-hole counts. The $d_{3/2}$ counts show a deviation from linearity which is probably due to a larger error associated with the much smaller values. From these observations it is not yet clear what role the change in number of Cu neighbors and the changing distances plays in charge redistribution. It can be stated that the decrease in interatomic distance seems to play a less important role than the coordination number of Au and Cu nearest neighbors: The latter is in line with electronegativity arguments. In addition, the increase in hole counts is linear upon increasing Cu concentration (thereby the number of Cu nearest neighbors) and the hole count is not increased further by a smaller Au-Cu distance. This can easily be clarified by comparing these results to the respective ordered species.

The lattice parameters for the ordered counterparts of Cu_3Au, AuCu, and Au_3Cu are 3.747, 3.865, and 3.980 Å,[53] respectively, which is, comparatively, a small reduction from the disordered species. Yet when examining the experimental data, there are large differences exhibited between these species in terms of XANES measurements, Mössbauer isomer shifts, and XANES- and XPS-derived d-hole counts. Smaller changes are noted for core-level shifts, and no changes can be observed in the d-band width and splitting because of the lowly resolved emission features of the alloy valence band at our experimental resolution. Figure 13 shows a large deviation from linearity, for the ordered species, which is not associated with a reduction in Au-Cu distance, but must be associated with a large change in the immediate environment of Au. For ordered Cu_3Au, Au has 12 Cu neighbors in the first shell as compared to 9 for disordered Cu_3Au. For ordered AuCu, Au has 8 Cu, neighbors in the first shell as compared to 6 for disordered AuCu. Finally, for ordered Au_3Cu, Au has 4 Cu neighbors in the first shell as compared to 3 for disordered Au_3Cu. In examining Fig. 13, an estimation of the number of nearest Cu neighbors for the ordered species can be determined by their hole counts. By extending the total hole count across to intercept a linear line that best fits the disordered and dilute Au species, the number of Cu nearest neighbors can be read off (i.e., 25% Cu corresponds to 3 Cu neighbors and 75% Cu corresponds to 9 Cu nearest neighbors). For Au_3Cu and AuCu, the estimation corresponds very well to the actual local Au environment. The exception is Cu_3Au, which has 12 Cu neighbors but has a lower hole count than the dilute Au species. Second-order effects come into play as the dilute Au samples have a higher number of Cu next-nearest neighbors (reducing the Au-Au interaction) than Cu_3Au, which has 6, and also interatomic distances may play a more important role since the fcc structure for these alloys is that of pure Cu.

The order and disorder Au_3Cu samples exhibit the same XAFS spectrum and have almost the same hole count, within experimental error, via both analysis methods. They also exhibit no difference in core-level shifts. We cannot, however, conclude that, upon annealing the disordered sample at 463 K for 2 weeks, it did not undergo a phase transition to an ordered state. With the highly concentrated Au samples, small changes to the number of Cu nearest neighbors (4 Cu neighbors for the ordered state versus 3 Cu neighbors for the disordered state) and Au nearest neighbors (8 versus 9) will not have a great effect on either the near-edge absorption or the core-level shifts.

The order and disorder AuCu samples show large differences in d-hole counts. Cu K-edge XANES spectra clearly show that the annealed sample has a higher occupied Cu $3d$ count (i.e., a gain of d charge at the Cu site because of increased Au-Cu interaction), and preliminary EXAFS analysis (Fig. 1) indicates a longer-range order exhibited by the annealed sample. The core-level shifts are also consistent, qualitatively, but the difference between the two samples is not as large as expected. This does show the advantage of XANES spectra in that they show more dramatic differences with small changes in the d states than do core-level shifts. Previous experimental

work indicates considerable differences in electronic structure with a larger bandwidth and more well-defined valence-band features for the ordered species.[54] Our present XPS work does not show such an apparent difference in the valence-band features, but the large differences in derived hole counts do support their conclusions. Calculations have been performed to evaluate the nature and the amount of charge transferred in an ordered AuCu alloy.[55] These calculations indicate a loss of 0.066 *d* electrons from the Au site and an overall gain of 0.176 *s-p* electrons (conduction) at the Au site upon alloying. These compare favorably with values determined in this study of 0.116 and 0.187 electrons, respectively.

A large body of work has been done experimentally on the Cu_3Au system. Recently, more theoretical work has appeared and will be the focus of comparison, as the experimental data agree well with previous studies. A *d*-band splitting parameter of 1.55 eV was calculated using the atomic spin-orbit splitting parameter $\frac{5}{2}\xi_d$ in which ξ was estimated to be 0.62.[27] The value derived from the XPS valence spectrum was also 1.55 eV. The same study gave a core-level shift of 0.3 eV, which compares well to a shift of 0.37 eV exhibited here. Calculated valence-band spectra also have shown more defined features for the ordered states[21,23,28] which were assigned to be due to a well-defined nearest-neighbor shell of 12 identical Cu atoms, which would allow resonant scattering, leading to more enhanced and defined features in the valence-band spectra.[23] Again, the resolution and cross section of the valence band prevented this study from seeing all but the most subtle of differences in the two alloys. There was also indication that the Au site gains 0.17 *d* electrons upon alloying.[21] However, the XANES results clearly indicate that Au loses *d* charge in direct contradiction with this study. A first-principles calculation has shown Au 5*d* loss of 0.21 and 0.17 electrons for the ordered and disordered species, respectively,[24] while a fast LMTO-CPA (linear-muffin-tin-orbital method using the coherent potential approximation) study indicated a loss of 0.43 and 0.22 electrons.[23] The values derived here were 0.16 and 0.13 electrons, in reasonable agreement with the first-principles study. The second study[23] also indicated that Au loses not only *d* charge, but also combined *s-p* charge, giving an overall loss of charge for both alloys in direct contradiction with the charge compensation model, electronegativity arguments, and the results of this study.

The last two samples analyzed were the random alloys $Au_{0.125}Cu_{0.875}$ and $Au_{0.05}Cu_{0.95}$. These can be viewed as having a pure Cu structure with Au atoms as impurities in the lattice. In both cases the first shell, statistically, would be dominated by Cu, and therefore the Au-Cu interaction from the Au viewpoint would be at its strongest and the Au-Au interaction at its weakest. These alloys exhibit the largest core-level and isomer shifts, have the highest hole count, and from the point of view of the charge compensation model they also have the largest overall gain of charge at the Au site, in good agreement with electronegativity arguments, albeit the amount being small to preserve electroneutrality. Second-order effects become important in these dilute alloys.

V. CONCLUSIONS

We have reported a wide range of experimental data of a series of Au-Cu alloys in order to elucidate trends in the electronic behavior upon alloying and ordering. Strong correlations have been found in the experimental parameters examined here (XPS, Mössbauer, and XANES). The sensitivity of the XANES technique has clearly been demonstrated and the validity of the charge compensation model shown by the independent determination of the nature and amount of charge transfer. Au gains overall charge, in line with electronegativity arguments. The degree of Au-Cu interaction is determined mainly by first-order local effects (number of Cu nearest neighbors) and not so much by the Au-Cu separation within the first coordination sphere. The results of this study compare favorably with most experimental and theoretical work, and although the valence-band spectra do not show the large differences associated with the transition between ordered and disordered samples, the XANES- and XPS-(core-level shifts) derived parameters clearly indicate significant differences in electron distribution.

With this study and that reported previously[29] the indication is that there is not much overlap between the constituent *d* bands, as indicated by the movement of the Au portion of the alloy band away from the Fermi level and the movement of the Cu portion toward the Fermi level (*d-d* reulsion model). Also, even as the significance of the Au-Cu interaction was stressed to point out differences that are associated with compositional and local environment changes, it must be noted that the overall synergy (redistribution) of charge is still relatively small.

This study has examined the electronic structure of a series of Au-Cu alloys and has confirmed the validity of the charge compensation model. The parameters and correlations derived from this bulk study will be used to determine the structure and electronic properties of bimetallic Au-Cu surface alloys.

ACKNOWLEDGMENTS

We are indebted to Walter Kunnmann of the Brookhaven National Laboratory for the preparation of the samples. Research carried out at the University of Western Ontario is supported by the Natural Science and Engineering Research Council (NSERC) of Canada and the Ontario Centre for Materials Research (OCMR). XAFS experiments were carried out at the X-11A beam line of the National Synchrotron Light Source (NSLS) at Brookhaven National Laboratory which is supported by the U.S. Department of Energy. XPS experiments were carried out at Surface Science Western at the University of Western Ontario. M.K. acknowledges the support of the NSERC.

[1]R. Fowler and E. A. Guggenheim, *Statistical Thermodynamics* (Cambridge University Press, London, 1949).
[2]H. Sato and R. S. Toth, Phys. Rev. **124**, 1833 (1961).
[3]P. G. Huray, L. D. Roberts, and J. D. Thomson, Phys. Rev. B **4**, 2147 (1971).
[4]T. K. Sham, R. E. Watson, and M. L. Perlman, Adv. Chem. Series **194**, ACS.39 (1981).
[5]T. K. Sham, Y. M. Yiu, M. Kuhn, and K. H. Tan, Phys. Rev. B **41**, 11 881 (1990).
[6]R. E. Watson, J. Hudis, and M. L. Perlman, Phys. Rev. B **4**, 4139 (1971).
[7]T. K. Sham, M. L. Perlman, and R. E. Watson, Phys. Rev. B **9**, 539 (1979).
[8]G. K. Wertheim, R. L. Cohen, G. Crecelius, K. W. West, and J. Wernick, Phys. Rev. B **20**, 860 (1979).
[9]P. M. Th. M. van Attekum, G. K. Wertheim, G. Crecelius, and J. H. Wernick, Phys. Rev. B **22**, 3998 (1980).
[10]W. Eberhardt, S. C. Wu, R. Garrett, D. Sondericker, and F. Jona, Phys. Rev. B **31**, 8285 (1985).
[11]V. L. Morruzzi, A. R. Williams, and J. F. Janak, Phys. Rev. B **10**, 4856 (1974).
[12]C. C. Tyson, A. Bzowski, P. Kristof, M. Kuhn, R. Sammynaiken, and T. K. Sham, Phys. Rev. B **45**, 8924 (1992); A. Bzowski and T. K. Sham (unpublished).
[13]A. Bzowski and T. K. Sham, J. Vac. Sci. Technol. A **11**, 2153 (1993).
[14]R. Sammynaiken, M. Kuhn, and T. K. Sham (unpublished).
[15]M. Kuhn, A. Bzowski, and T. K. Sham (unpublished).
[16]A. Bzowski, K. Kuhn, and T. K. Sham (unpublished).
[17]J. A. Catterall and J. Trotter, Proc. Phys. Soc. London **79**, 691 (1962).
[18]S. B. DiCenzo, P. H. Citrin, E. H. Hartford, Jr., and G. K. Wertheim, Phys. Rev. B **34**, 1343 (1986).
[19]G. K. Wertheim, Phys. Rev. B **36**, 4432 (1987).
[20]T. K. Sham, A. Bzowski, M. Kuhn, and C. C. Tyson, Solid State Commun. **80**, 29 (1991).
[21]G. K. Wertheim, L. F. Mattheiss, and D. N. E. Buchanan, Phys. Rev. B **38**, 5988 (1988).
[22]B. Ginatempo, G. Y. Guo, W. M. Temmerman, J. B. Staunton, and P. J. Durham, Phys. Rev. B **42**, 2761 (1990).
[23]I. A. Abrikosov, Yu.H. Vekilov, and A. V. Ruban, Phys. Lett. A **154**, 407 (1991).
[24]Z. W. Lu, S.-H. Wei, and A. Zunger, Phys. Rev. B **45**, 10 314 (1992).
[25]A. Stuck, J. Osterwalder, T. Greber, S. Hüfner, and L. Schlapbach, Phys. Rev. Lett. **65**, 3029 (1990).
[26]G. S. Sohal, C. Carbone, E. Kisker, S. Krummacher, A. Fattah, W. Uelhoff, R. C. Albers, and P. Weinberger, Z. Phys. B **78**, 295 (1990).
[27]J. W. Davenport, R. E. Watson, and M. Weinert, Phys. Rev. B **37**, 9985 (1988).
[28]P. Weinberger, A. M. Boring, R. C. Albers, and W. M. Temmerman, Phys. Rev. B **38**, 5357 (1988).
[29]M. Kuhn, T. K. Sham, J. M. Chen, and K. H. Tan, Solid State Commun. **75**, 861 (1991).
[30]L. M. Mattheiss and R. E. Dietz, Phys. Rev. B **22**, 1663 (1980).
[31]N. F. Mott, Proc. Phys. Soc. London A **62**, 416 (1949).
[32]Y. Caucchois and I. Manescu, C. R. Acad. Sci. **210**, 172 (1940).
[33]D. Coster and H. De Lang, Physica **15**, 351 (1949).
[34]M. Brown, R. E. Peierls, and E. A. Stern, Phys. Rev. B **15**, 738 (1977).
[35]F. W. Lytle, P. S. P. Wei, R. B. Greegor, G. H. Via, and J. H. Sinfelt, J. Chem. Phys. **70**, 4849 (1979).
[36]A. N. Mansour, J. W. Cook, Jr., and D. E. Sayers, J. Phys. Chem. **88**, 2330 (1984).
[37]T. Claeson and J. B. Boyce, Phys. Rev. B **29**, 1551 (1984).
[38]P. M. Hansen, *Constitution of Binary Alloys,* 2nd ed. (McGraw-Hill, New York, 1958).
[39]J. E. Müller, O. Jepsen, and J. W. Wilkins, Solid State Commun. **42**, 365 (1987).
[40]T. K. Sham, A. Hiraya, and M. Watanabe (unpublished).
[41]R. E. Watson and M. L. Perlman, Phys. Scr. **21**, 529 (1980).
[42]R. M. Friedman, J. Hudis, M. L. Perlman, and R. E. Watson, Phys. Rev. B **8**, 2433 (1973).
[43]F. Cyrot-Lackmann, Adv. Phys. **16**, 393 (1967).
[44]M. Kuhn, Z. H. Lu, and T. K. Sham, Phys. Rev. B **45**, 3703 (1992).
[45]B. K. Teo and A. P. Lee, J. Am. Chem. Soc. **101**, 2815 (1979).
[46]W. H. McMaster, N. K. Del Grande, J. Mallett, and J. H. Hubbell, *Compilation of X-ray Cross-Sections* (NTI Service, Springfield, VA, 1969).
[47]L. D. Roberts, R. L. Becker, F. E. Obenshain, and J. O. Thomson, Phys. Rev. **137**, A895 (1965).
[48]R. L. Cohen, in *Mössbauer Isomer Shifts,* edited by G. K. Shenoy (North-Holland, Amsterdam, 1978), p. 541.
[49]R. M. Friedman, J. Hudis, M. L. Perlman, and R. E. Watson, Phys. Rev. B **19**, 539 (1979).
[50]T. S. Chou, M. L. Perlman, and R. E. Watson, Phys. Rev. B **14**, 3248 (1976).
[51]M. Kuhn and T. K. Sham (unpublished).
[52]L. G. Parratt, Rev. Mod. Phys. **16**, 393 (1967).
[53]S. S. Lu and C.-K. Liang, Chin. J. Phys. **22**, 505 (1966).
[54]R. G. Jordan, A. M. Begley, Y. Jiang, and M. A. Hoyland, J. Phys. Condens. Matter **3**, 1685 (1991).
[55]S.-H. Wei, A. A. Mbaye, L. G. Ferreira, and A. Zunger, Phys. Rev. B **36**, 4163 (1987).